Acousto-Plasmonic and Surface-Enhanced Raman Scattering Properties of Coupled Gold Nanospheres/Nanodisk Trimers

ARTICLE *in* NANO LETTERS · FEBRUARY 2011

Impact Factor: 13.59 · DOI: 10.1021/nl103089e · Source: PubMed

10 AUTHORS, INCLUDING:

Sudhiranjan Tripathy
Agency for Science, Technology and Researc…
237 PUBLICATIONS **2,716** CITATIONS
SEE PROFILE

Vivian Kaixin Lin
Agency for Science, Technology and Researc…
25 PUBLICATIONS **304** CITATIONS
SEE PROFILE

Arnaud Arbouet
Centre d'Élaboration de Matériaux et d'Etud…
79 PUBLICATIONS **951** CITATIONS
SEE PROFILE

Adnen Mlayah
Paul Sabatier University - Toulouse III
106 PUBLICATIONS **1,427** CITATIONS
SEE PROFILE

NANO LETTERS

LETTER

pubs.acs.org/NanoLett

Acousto-Plasmonic and Surface-Enhanced Raman Scattering Properties of Coupled Gold Nanospheres/Nanodisk Trimers

Sudhiranjan Tripathy,*[,†] Renaud Marty,[‡] Vivian Kaixin Lin,[†] Siew Lang Teo,[†] Enyi Ye,[†] Arnaud Arbouet,[‡] Lucien Saviot,[§] Christian Girard,[‡] Ming Yong Han,*[,†] and Adnen Mlayah*[,‡]

[†]Institute of Material Research and Engineering, A*STAR, 3 Research Link, 117602 Singapore

[‡]Centre d'Elaboration de Matériaux et d'Etudes Structurales CNRS—Université de Toulouse, 29 Rue J. Marvig, 31055 Toulouse, France

[§]Laboratoire Interdisciplinaire Carnot de Bourgogne CNRS—Université de Bourgogne, 9 Av. A. Savary, 21078 Dijon, France

Supporting Information

ABSTRACT: This work is devoted to the fundamental understanding of the interaction between acoustic vibrations and surface plasmons in metallic nano-objects. The acoustoplasmonic properties of coupled spherical gold nanoparticles and nanodisk trimers are investigated experimentally by optical transmission measurements and resonant Raman scattering experiments. For excitation close to resonance with the localized surface plasmons of the nanodisk trimers, we are able to detect several intense Raman bands generated by the spherical gold nanoparticles. On the basis of both vibrational dynamics calculations and Raman selection rules, the measured Raman bands are assigned to fundamental and overtones of the quadrupolar and breathing vibration modes of the spherical gold nanoparticles. Simulations of the electric near-field intensity maps performed at the Raman probe wavelengths showed strong localization of the optical energy in the vicinity of the nanodisk trimers, thus corroborating the role of the interaction between the acoustic vibrations of the spherical nanoparticles and the surface plasmons of the nanodisk trimers. Acoustic phonons surface enhanced Raman scattering is here demonstrated for the first time for such coupled plasmonic systems. This work paves the way to surface plasmon engineering for sensing the vibrational properties of nanoparticles.

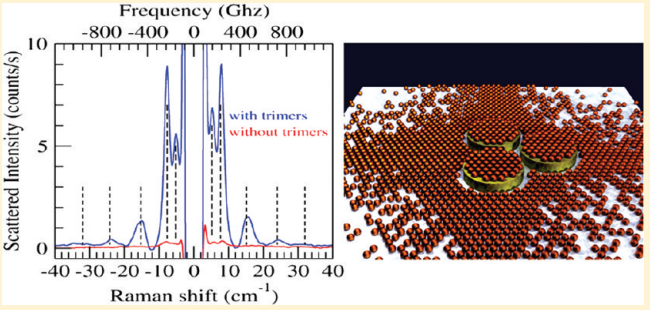

KEYWORDS: Surface plasmon resonance, acoustic vibrations, nanoparticle, oligomer, Raman scattering, SERS

The optical properties of noble metal nano-objects rely on the collective oscillations of their free electron cloud, namely, the surface plasmons. Light absorption and scattering are greatly influenced by the dependence of the surface plasmons on the size and shape of the nano-objects and on the electromagnetic interaction between nano-objects.[1−7] The engineering of the surface plasmon properties has led to several new applications such as subwavelength optical imaging,[8−10] biochemical and chemical sensing,[11−14] in vivo cancer cell imaging, and hyperthermia cancer treatment.[15,16] Basically, the interest in metal nano-objects lies in their ability to concentrate the electromagnetic energy at visible wavelengths (a few hundreds of nanometers) on dimensions comparable to their size (from a few nanometers to a few tens of nanometers), thus leading to strong electric near-field enhancement. This effect has been exploited for amplifying elastic (Rayleigh) and inelastic (Raman) light scattering processes. In particular, surface-enhanced Raman scattering (SERS) has been intensively studied these last 20 years[17−19] and has recently been used for selective spectroscopic imaging of cancer cells.[20,21] So far, SERS has been reported mostly for scattering by intramolecular optical vibrations which occur at high frequencies (a few hundreds to a few thousands of wavenumbers).

In this work, we report on SERS occurring in the 2−50 cm^{-1} spectral region, where scattering is due to acoustic vibrations of nanostructures.[22−24] Raman scattering by acoustic vibrations of metal nano-objects has been addressed in several reports. In particular, the size and shape dependence of the acoustic vibrations and their related Raman activity have been the subject of detailed experimental and theoretical investigations.[22−29] However, in most of the previously reported works, the scattering was excited in resonance with the surface plasmons of the nano-objects *themselves*. Hence, all established Raman activities and selection rules assume coupling between acoustic vibrations and surface plasmons of the *same* nano-object. But are these selection rules still valid when considering the interaction between acoustic vibrations of spherical nanoparticles and surface plasmons that do not exhibit any spherical symmetry? Could we control the acoustic phonons SERS (AP-SERS) effect by engineering the surface plasmons? Answering these questions requires separating the vibrational dynamics and the surface plasmon properties.

Received: September 1, 2010
Revised: December 17, 2010
Published: January 7, 2011

This can be achieved by allowing for acousto-plasmonic interaction between two different systems, one providing the acoustic vibrations and the other the surface plasmons. In a previous work,[29] some of us showed that Raman scattering by acoustic vibrations of Co nanoparticles, which lack sharp optical transitions, can indeed be enhanced using surface plasmon resonance of silver nanoparticles. Inspired by this idea, we demonstrate in this work an unprecedented monitoring of the interaction between surface plasmons and acoustic vibrations.

The studied system combines spherical gold nanoparticles, from a colloidal solution, and gold nanodisk trimers processed by electron beam lithography. The acoustic vibrations of the spherical nanoparticles are revealed by low-frequency Raman scattering. The Raman probe wavelengths are chosen to selectively excite the surface plasmons of either the nanoparticles or the nanodisk trimers. The electromagnetic interaction among the gold nanodisks in the trimer configuration provides the localized electric near-fields at the origin of the AP-SERS. The work shed light on the acousto-plasmonic interaction in metal nano-objects and provides a method for sensing the vibrational properties of nanoparticles.

Oleylamine-coated gold nanoparticles of 13 nm in diameter were chemically synthesized and used for coating the gold nanodisk trimers (details on the synthesis are given in section S1 of the Supporting Information). Figure 1 shows the transmission electron microscopy (TEM) and the high-resolution TEM (HR-TEM) of the gold nanoparticles (NPs) which are nearly monodisperse and monocrystalline (inset of Figure 1). Furthermore, the hydrophobic nature of these oleylamine-coated gold nanoparticles leads to the formation of a uniform self-assembly via hydrophobic−hydrophobic interaction among gold particles. The NPs are organized in a hexagonal lattice, and the separation between adjacent gold nanoparticles is about 2 nm. The hydrophobic nature of the oleylamine coating allows the gold NPs to self-assemble on the hydrophobic gold nanodisk trimers which were fabricated on a hydrophilic quartz substrate.

Figure 1 shows a typical scanning electron microscopy (SEM) image of nanodisk trimers (NDTs) used to generate AP-SERS. The average nanodisk height and diameter are 29 ± 1 and 125 ± 2 nm, respectively, and the gap between disk edges varies between 10 and 14 nm in various trimer samples. Three periods, i.e., axis to axis separation (S) between trimers, have been used in the present work: S = 0.4, 1, and 2 μm. All three patterns were processed on the same sample. Nanodisk trimers were preferred to single nanodisks and dimers because they provide a larger optical volume (i.e., a larger optical density) while preserving sharp surface plasmon resonances in the red spectral range and strong confinement of the electromagnetic field that can be controlled by the separation between the nanodisks.[14] Moreover, the size and spacing between nanodisks in the trimers used in this study provide SPR features that are suitable for resonant excitation of the Raman scattering (given the available laser lines).

Since Raman scattering is here excited close to resonance with the SPRs, it is important to fully characterize the surface plasmon properties of the NPs and the NDTs as well as the interaction between the two systems. Figure 2 presents the optical density (OD) spectra recorded from the gold nanoparticles and from the NDTs using transmission measurements. For S = 0.4 μm, the NDT spectrum shows intense SPR around 660 nm. The spectrum simulated using the Green dyadic tensor formalism[30] is in good agreement with the measured one; a 14 nm air gap between the disks was used in order to reproduce the observed SPR

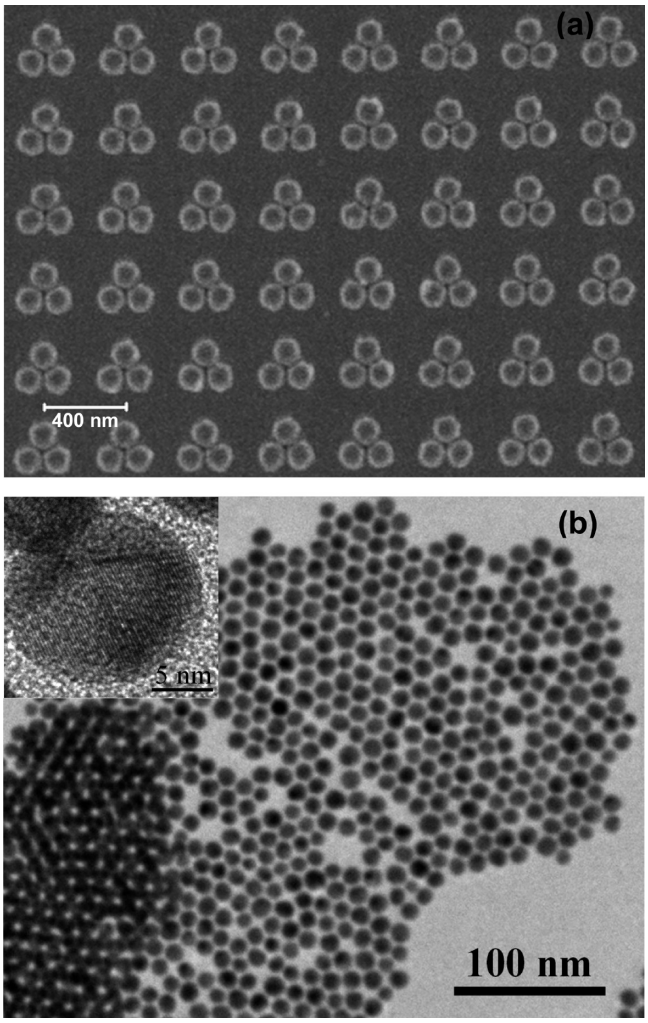

Figure 1. (a) SEM image of the gold nanodisk trimers fabricated by electron-beam lithography, thermal evaporation, and lift-off techniques. The disk average diameter is 125 ± 2 nm, and the separation between trimers (center to center) is about 400 nm. (b) TEM image of the oleylamine-coated gold nanoparticles. The average particle size is about 13 nm. The HR-TEM image (inset) shows a single crystal domain nanoparticle.

wavelength. For larger separation between trimers, S = 1 and 2 μm, the SPR resonance is much weaker due to the smaller number of trimers at the probe light focus (see section S2 of the Supporting Information). Transmission measurements from different points of the processed array showed good homogeneity of the disk trimers characteristics.

The optical density spectra of the gold NPs are also shown in Figure 2. The spectrum from the colloidal solution (Figure 2c) exhibits the 522 nm SPR typical of individual spherical gold nanoparticles and is well reproduced by the simulations. We have also collected the spectrum (Figure 2d) from a NP layer formed by coating the NPs colloidal solution on a quartz substrate. As can be noticed, the SPR is broader and is red-shifted to 562 nm compared to the SPR of individual NPs because of electromagnetic interactions between the nanoparticles.[31] This is confirmed by the theoretical simulations: the OD spectrum calculated for a network of 300 interacting gold NPs that mimic the self-assembly observed by TEM (including NPs size fluctuations) accounts well for the experimental SPR wavelength and bandwidth.

dx.doi.org/10.1021/nl103089e |*Nano Lett.* 2011, 11, 431–437

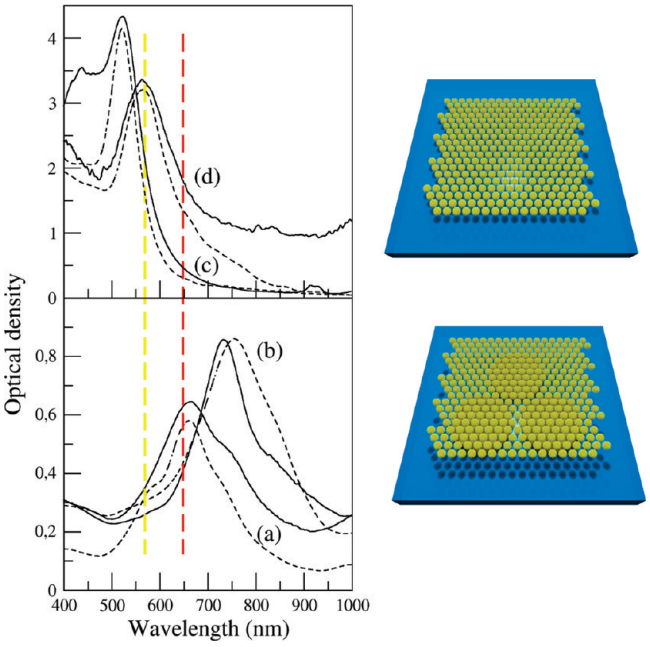

Figure 2. Upper panel: Optical density spectra of the gold nanoparticles from the colloidal solution (c) and from a NP layer coated on a glass substrate (d). The dashed lines show the spectra calculated for gold NPs in the colloidal solution and for a monolayer of 300 NPs self-assembled in a hexagonal lattice on a glass substrate as sketched in the upper right part of the figure. The self-assembly characteristics were taken from the TEM, and the separation between the NPs layer and the NDTs was 2 nm. Lower panel: Optical density spectra from the bare nanodisk trimers (a) and after coating with gold nanoparticles (b). The dashed lines show the spectra simulated for a trimer consisting of 125 ± 2 nm disks separated by 14 nm (edge to edge) air gap without (a) and with (b) the NPs layer coating. The latter situation is sketched in the lower right part of the figure. All spectra were recorded with unpolarized light. To simulate this experimental situation, the calculated spectra were averaged over several orientations of the incident polarization. Their intensity was then rescaled to allow for comparison with the measured ones. The vertical dashed lines show the yellow (568.2 nm) and red (647.1 nm) laser lines used for excitation of the Raman scattering.

In Figure 2, we have also shown the optical density spectrum of the NDTs coated with the gold NPs. The formed NP layer was much thinner and optically less dense than the one used to obtain the extinction spectrum (d) in Figure 2. As expected, the surface plasmon resonance of the NDTs is now red-shifted to 720 nm due to the well-known sensitivity of the SPR to the optical index of the surrounding medium. Such a red-shift has allowed for sensing of nanoparticles in plasmonic antenna[32] and is due to the interaction between the NPs and the NDTs in our case. The observed red shift is well reproduced by the simulations performed for a self-assembled NP layer on top of the NDTs (Figure 2). Hereafter we refer to the 720 nm resonance as the NPs@NDTs SPR.

Low-frequency Raman scattering was excited using the yellow and red lines (568.2 and 647.1 nm, respectively) of a krypton laser close the SPR of either the NPs layer or the NPs@NDTs system (Figure 2). It is worthwhile to mention that we have also used the 750 nm line which is very close to the NPs@NDTs SPR (see Figure.2). But, with this excitation line we observed a rapid degradation of the NPs layer due to plasmonic heating of the NDTs even at low incident laser intensities. In all Raman

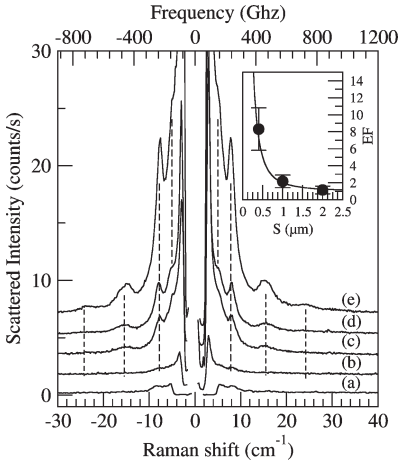

Figure 3. Stokes and anti-Stokes low-frequency Raman scattering from the gold nanoparticles layer outside (spectra a and b) and inside (spectra c, d, and e) the nanodisk trimers area. Spectrum a was excited using the yellow laser line (568.2 nm), i.e., in resonance with the surface plasmons of the NP layer on quartz (shown in Figure 2). Spectra b−e were excited using the red laser line (647.1 nm) close to the resonance of the nanodisk trimers with NPs on top. Spectra c, d, and e were collected with laser spots focused on the nanodisk trimers separated by S = 2, 1, and 0.4 μm, respectively. All spectra are unanalyzed, i.e., integrated over all scattered polarizations. The vertical dashed lines highlight the frequencies of the measured Raman bands. The inset shows the enhancement factor EF of the 7.7 cm^{-1} Raman peak as a function of the separation S between the trimers (dots). The intensity of the 7.7 cm^{-1} Raman signal, visible in spectrum a, was used as a reference for estimation of the enhancement factor. The continuous line in the inset shows the $1/S^2$ dependence.

experiments the laser intensity was fixed at 0.5 mW/μm^2 at the focal plane. The scattered light was collected through a 50× objective of a confocal microscope with 0.8 numerical aperture and dispersed using a spectrometer which allows for high rejection of the Rayleigh scattering. The laser spot size is about 10 μm^2 and the incidence angle is 60° with respect to the normal of the sample surface. From the optical density of the NPs colloidal solution, and assuming that the deposited volume uniformly covered the entire sample area, we estimate that around 8000 nanoparticles are present under the laser spot. However, during evaporation of the solvent, the NPs agglomerate and self-organize and their surface density could be locally much larger than the 8000/10 μm^2, thus leading to the formation of NP layer stacks. We have observed that the deposited layer was uniformly covering the NDT patterns (S = 0.4, 1, and 2 μm) and a large region around the patterns. Different points inside and outside the NDTs patterned regions were probed in order to check the reproducibility and uniformity of the results. We estimate that stacks of approximately two monolayers of self-organized NPs were present under the laser spot. Furthermore, no Raman signal was detected from the bare NDTs whatever the excitation line.

Figure 3 presents the Stokes and anti-Stokes low-frequency Raman spectra recorded close to the NPs@NDTs SPR and for the three periods S = 0.4, 1.0, and 2.0 μm. Also shown are the spectra collected from focus points outside the NDT area (i.e., where only self-assembled NPs are present). In that case both yellow and red excitation lines were used.

First, one can notice that Raman scattering from the NPs located outside the NDT area is very weak for both yellow and red excitations (spectra a and b in Figure 3). This is due to the

dx.doi.org/10.1021/nl103089e |Nano Lett. 2011, 11, 431–437

rather small number of NPs under the laser spot (around 8000). Moreover, the red excitation line is resonant neither with the SPR of individual NPs nor with that of the self-assembled NPs layer as shown in Figure 2. On the contrary, for yellow excitation, the surface plasmons of the NPs layer could be resonantly excited (Figure 2) and a weak Raman peak around 7.7 cm^{-1} is indeed detected in both Stokes and anti-Stokes regions (spectrum a in Figure 3).

Second, let us consider the situation where the laser spot is focused inside the NDT area and the Raman excitation is close to resonance with the SPR of the NPs@NDTs (i.e., red excitation in Figure 2). For 2 μm separation between the NDTs, the Raman signal around 7.7 cm^{-1} becomes clearly visible and an additional peak appears around 15 cm^{-1} (spectrum c in Figure 3). This signal increases for 1 μm separation (spectrum d in Figure 3) and becomes even more intense for 0.4 μm separation (spectrum e in Figure 3). In this case, at least five Raman peaks are detected around 5.2, 7.7, 15, 23, and 30 cm^{-1}. The measurements were performed at several focus points inside the NDTs area and showed good reproducibility. By comparing the Raman intensities measured outside and inside the NDTs area (spectra e and b) and given the scattered intensity increase with decreasing separation between the NDTs, we assign the observed Raman scattering to AP-SERS involving acoustic vibrations of the spherical gold NPs and their interaction with the surface plasmons of the nanodisk trimers.

Third, using Lorentzian line shape fitting to the measured Raman spectra, we extracted the Raman intensities and estimated the enhancement factor. The Raman scattering from the NPs located outside the NDT area, and excited with the red line (i.e., out of resonance), is very weak (spectrum b in Figure 3) as compared to the intensities measured for the NPs@NDTs (spectrum e in Figure 3). The corresponding enhancement factor averaged on both Stokes and anti-Stokes intensities at 7.7 cm^{-1} is around 43. Moreover, it is interesting to address the contribution of the NDTs to the Raman gain with respect to the one generated by the surface plasmons of the interacting nanoparticles. Hence, we use the Raman signal measured outside the NDTs with the yellow line as a reference (spectrum a in Figure 3). In doing so, we obtain the enhancement due to the nanodisk trimers with respect to the one produced by the interaction between the nanoparticles within the self-assembly.

The so-defined enhancement factor (EF), averaged on both Stokes and anti-Stokes intensities at 7.7 cm^{-1}, is shown in the inset of Figure 3 as a function of the separation between NDTs. As can be seen, the EF increases with decreasing separation between NDTs up to a maximum value of 8.3 for $S = 0.4$ μm. In the case of AP-SERS produced by acoustic vibrations of gold NPs interacting with surface plasmons of the nanodisk trimers, one expects the Raman signal to increase linearly with the number, N_{NDT}, of nanodisk trimers at the laser spot. Hence, EF should be proportional to $N_{NDT} = S_{laser}/S^2$, where S_{laser} is the laser spot area and S^2 is the unit surface defined by the NDTs separation S. In the inset of Figure 3 is plotted the $1/S^2$ variation; a very good agreement with the measured EF values is obtained, thus corroborating the role of the NDTs in the observed AP-SERS. For $S = 0.4$ μm, we have $N_{NDT} \approx 63$ leading to an enhancement factor of 13% per trimer with respect to the resonant Raman scattering from the NPs self-assembled layer (spectrum a in Figure 3).

In order to assign the Raman features to the acoustic vibration modes of the gold nanoparticles, we have investigated the Raman selection rules and performed vibrational dynamics calculations. The Raman spectra recorded for both parallel (VV) and crossed (HV) incident and scattered polarizations are shown in Figure 4.

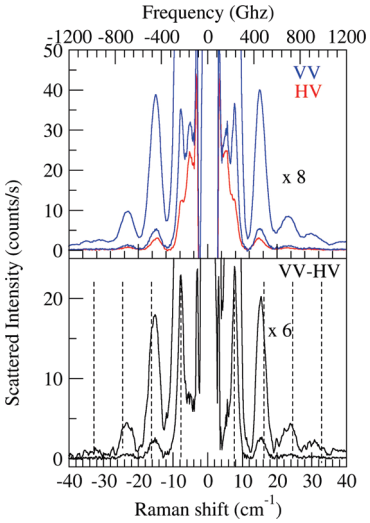

Figure 4. Upper panel: low-frequency Raman scattering by acoustic vibrations of the gold nanoparticle layer coated on the NDTs, recorded in the crossed (HV) and parallel (VV) incident and scattered polarizations and excited with the 647.1 nm laser line. The spectra were corrected for Rayleigh scattering. The separation between the NDTs is $S = 0.4$ μm. The incident electric field is either in the incidence plane (V, P-polarization) or perpendicular to the incidence plane (H, S-polarization). The VV spectrum is also shown with a ($\times 8$) magnification. Lower panel: difference between VV and HV spectra. The difference spectrum is also shown with a ($\times 6$) magnification, thus clearly revealing the scattering by the ($n = 1, 2, 3, 4, l = 0$) breathing vibrations of the gold NPs. The vertical dashed lines show the calculated frequencies of the breathing vibration modes.

It is well-known that the Raman active vibrations of a spherical metal nanoparticles are the quadrupolar (n, $l = 2$) and the breathing (n, $l = 0$) modes, where n and l are integers that label the mode order and angular momentum, respectively. The quadrupolar vibration modes give rise to depolarized Raman scattering (i.e., contribute to both crossed and parallel configurations), whereas scattering by breathing modes is totally polarized (i.e., visible in the parallel configuration only).[24,25,28] Therefore, the (VV−HV) spectra shown in Figure 4 reveal the contribution of breathing modes, whereas the (HV) spectrum is due to quadrupolar modes. Owing to the large enhancement of the Raman scattering provided by the NDTs, we are able to observe (Figure 4) four quadrupolar modes at 5.2, 14.7, 22.6, and 29 cm^{-1} and four breathing modes at 7.7, 15.2, 23.2, and 30 cm^{-1} of different orders.

The Raman selection rules allow for identifying the nature of the vibration modes (either quadrupolar or breathing). To determine the order of each observed mode, we have performed vibrational dynamics calculations and used the dependence of the vibration eigen frequencies on the nanoparticle size. Details on the calculation methods and results are given as Supporting Information (section S3). As shown in Figure 4, a very good agreement between calculated and measured vibration frequencies is obtained for a 13.5 nm gold nanoparticle which is perfectly matching the average nanoparticle size deduced from TEM (13 nm). Moreover, we can identify breathing vibration modes up to the fourth order in the (VV−HV) Raman spectrum (Figure 4).

dx.doi.org/10.1021/nl103089e |*Nano Lett.* 2011, 11, 431–437

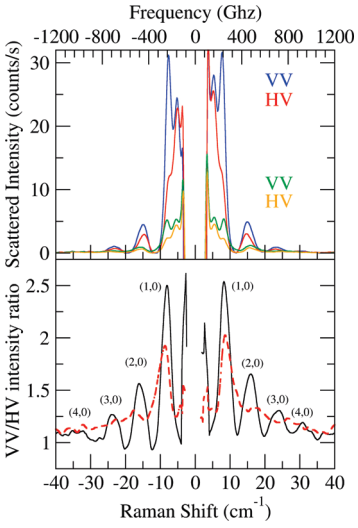

Figure 5. Upper panel: low-frequency Raman spectra recorded in the parallel (VV) and crossed (HV) scattering configurations from the NPs located on the NDTs (blue and red plots) and from a high density NPs layer coated on quartz (green and orange plots). All spectra were excited using the red excitation line 647.1 nm and corrected for Rayleigh scattering. Lower panel: VV/HV Raman intensity ratios obtained for the NPs on NDTs (continuous line) and for the NPs on quartz (red dashed line). In order to avoid divergence of the ratios, due to zero values of the HV intensities, all measured intensities were shifted by 1.

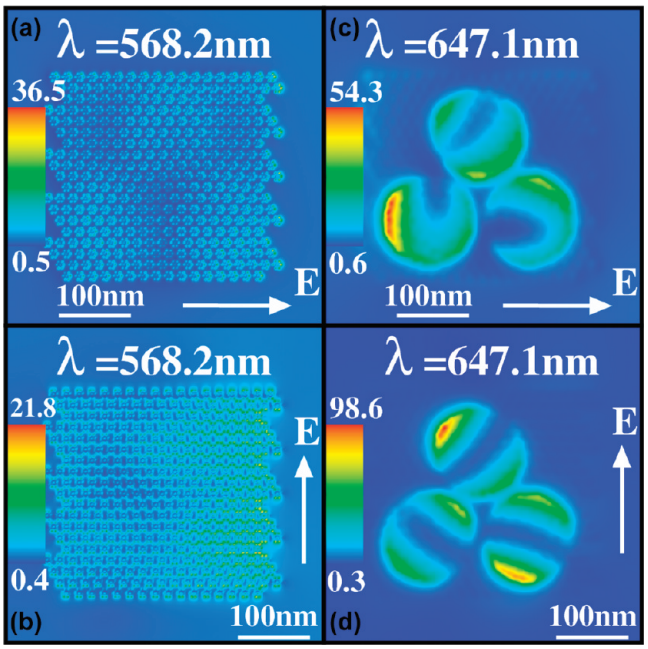

Figure 6. Simulated intensity maps of the electric field generated by the Raman probe at 568.2 nm (left: (a) and (b)) and 647.1 nm (right: (c) and (d)) for the NP layer on NDT (sketched in Figure 2). The excitation field is allowed to shine onto the NPs on the NDT system under 60° incidence angle with either P (top: (a) and (c)) or S (bottom: (b) and (d)) polarizations. The quartz substrate is taken into account in the simulations. The electric field has been mapped at 5 nm above the NPs layer, i.e., 20 nm above the nanodisks. At this altitude, dipole-like electric near-field distributions mainly localized at the edges of the nanodisks are observed. The symmetry of the electric-field patterns at 647.1 nm reflects the interaction between the NDTs and between the NDTs and the NPs layer.

Now that the Raman features have been identified, an interesting question can be raised concerning the Raman selection rules: Are the relative Raman activities of the acoustic vibration modes modified by the nanodisk trimers or is the AP-SERS effect producing a global increase of the scattered intensity?

To address this issue, we compare in Figure 5 the Raman spectra of the NPs on NDTs (spectra of Figure 4) and of the NPs on quartz excited at the same wavelength (red line). Given the weak Raman scattering from the NPs located outside the NDTs area and excited with the red line (spectrum b in Figure 3), we used a high optical density NP layer in order to increase the signal and to allow for determining the Raman selection rules in the absence of the NDTs. One must indeed keep in mind that the red excitation is away from the NPs SPR (Figure 2) and their Raman signal is therefore very weak.

As can be noticed in Figure 5, similar enhancements are obtained in the parallel (VV) and crossed configurations (HV). In Figure 5 are also plotted the VV/HV intensity ratios (we have added a value of 1 to all measured intensities in order to avoid divergence due to zeros in the Rayleigh corrected HV spectra). The VV/HV ratio gives the relative Raman intensities of breathing and quadrupolar vibration modes. No contribution from breathing vibrations gives VV/HV = 1. Similarly to the observation in Figure 4, breathing vibration modes up to the fourth order clearly appear as maxima of the VV/HV intensity ratio for the NPs on NDTs. For the NPs on quartz, apart from the fundamental breathing mode (n = 1, l = 0), higher order modes are hardly detected; they are usually observed for resonant excitation of the nanoparticle surface plasmons as reported in previous works.[24,25] The VV/HV intensity ratio shows that the Raman scattering by breathing vibrations decreases more rapidly with increasing mode order for the NPs on quartz than for the NPs on NDTs. This means that scattering by overtones (n = 2, 3, 4) of the fundamental breathing mode is enhanced by the NDTs surface plasmons as compared to the case of NPs without NDTs. It should be noticed that different enhancement factors for totally symmetric vibration modes compared to nontotally symmetric ones is not specific to AP-SERS. The same difference has already been reported for SERS due to molecular vibrations and was ascribed to the different coupling strength in the SERS process.[34]

To go deeper into the understanding of the AP-SERS effect, we have calculated the spatial distribution of the electric field intensity generated by the Raman probe. In order to mimic the experimental situation, we consider the model system sketched in Figure 2 in which all the plasmonic interactions are taken into account: interactions between the nanodisks forming the trimer, between the nanoparticles within the NPs layer and between the nanoparticles and the nanodisk trimer. The electric field $\mathbf{E}(\mathbf{r}, \lambda)$ at point $\mathbf{r}$ and excitation wavelength λ is computed from Lippmann−Schwinger's equation.[30,33] Figure 6 shows the electric near-field intensity maps computed for both the yellow and red excitations and for S and P incident polarizations corresponding to HV and VV configurations, respectively. The electric field is mapped at 5 nm above the NPs layer.

For the yellow excitation, the Raman probe is resonant with the surface plasmons of the self-assembled NPs layer (Figure 2d) and the electric near-field intensity maps (Figure 6) reveal that only the NPs are excited. The NDTs are almost invisible at this excitation wavelength (Figure 6, panels a and b) and play no role in the Raman scattering. In that situation the Raman scattering is

dx.doi.org/10.1021/nl103089e |Nano Lett. 2011, 11, 431–437

only due to the interaction between the NPs acoustic vibrations and their resonantly excited surface plasmons (spectrum a in Figure 3). In contrast, for red excitation, surface plasmons of the NPs@NDTs are effectively excited (Figure 6, panels c and d). On the contrary, the NPs are hardly seen in the intensity maps (Figure 6, panels c and d) and their surface plasmons play no role in the Raman scattering. The NPs located at the hot spots of the NDTs electric near-fields (Figure 6, panels c and d) give the strongest contribution to the Raman scattering. This confirms that the observed enhancement of the Raman scattering (Figures 3 and 5) is due to interaction between the acoustic vibrations of the spherical NPs and the surface plasmons of the nanodisk trimers. Moreover, those nanoparticles experience a nonuniform electric field with no particular symmetry which may enhance the Raman scattering by breathing vibrations.[27] Furthermore, one can notice in Figure 6 that the electric near-field intensities generated at the NDTs for S- and P-polarized Raman probe are very similar, thus explaining the comparable enhancements observed for VV and HV configurations (Figure 5).

In summary we have successfully measured the vibrational properties of 13 nm gold nanoparticles using nanofabricated plasmonic resonators. The acousto-plasmonic interaction between gold nanoparticles and nanodisk trimers was investigated using resonant Raman scattering, optical absorption measurements, and simulations of the vibrational dynamics and surface plasmon properties of this complex system. Owing to the good reproducibility of the electron beam lithographed nanodisk trimers, we obtained sharp surface plasmon resonances that we used as a means for enhancing the low-frequency Raman scattering by acoustic vibrations of the gold nanoparticles. The comparison between the Raman scattered intensities recorded with and without the NDTs, and the Raman intensity variation with density of the NDTs, both pointed out a strong enhancement effect. The simulations of the surface plasmon properties of the interacting NPs/NDTs system showed that this effect is connected with the hot spots in the electric near-field intensity distribution of the nanodisk trimers. The maximum enhancement factor was estimated around 8 (with respect to resonance with the self-assembled NPs layer SPR) and was high enough to allow for the observation of eight Raman bands. It is worthwhile to underline that Raman scattering by acoustic vibration overtones is usually observed for resonant excitation of the surface plasmons of the nanoparticles,[24,25] i.e., for blue or green excitation depending on the metal (silver or gold). Here we reported, for the first time, the observation of such scattering for red excitation. We have demonstrated the use of surface plasmons for intensifying the Raman scattering by acoustic vibrations, allowing the mechanical properties of nanoparticles to be probed.

■ ASSOCIATED CONTENT

Supporting Information. Synthesis of gold nanoparticles, optical spectra of bare gold nanodisk trimer samples with different pitch, and vibrational dynamics calculation methods. This material is available free of charge via the Internet at http://pubs.acs.org.

■ AUTHOR INFORMATION

Corresponding Author

*E-mail: tripathy-sudhiranjan@imre.a-star.edu.sg; my-han@imre.a-star.edu.sg; Adnen.Mlayah@cemes.fr.

■ ACKNOWLEDGMENT

The authors would like to thank funding support from the Agency for Science, Technology and Research (A*STAR) Singapore and French Embassy MERLION Program. This work was also supported by CALMIP computing facilities at Paul Sabatier University of Toulouse.

■ REFERENCES

(1) Maier, S. A.; Brongersma, M. L.; Kik, P. G.; Meltzer, S.; Requicha, A. A. G.; Atwater, H. A. *Adv. Mater.* **2001**, *13*, 1501–1505.

(2) Kabashin, A. V.; Evans, P.; Pastkovsky, S.; Hendren, W.; Wurtz, G. A.; Atkinson, R.; Pollard, R.; Podolskiy, V. A.; Zayats, A. V. *Nat. Mater.* **2009**, *8*, 867–871.

(3) Lal, S.; Grady, N. K.; Kundu, J.; Levin, C. S.; Lassiter, J. B.; Halas, N. J. *Chem. Soc. Rev.* **2008**, *37*, 898–911.

(4) Fan, J. A.; Wu, C. H.; Bao, K.; Bao, J. M.; Bardhan, R.; Halas, N. J.; Manoharan, V. N.; Nordlander, P.; Shvets, G.; Capasso, F. *Science* **2010**, *328*, 1135–1138.

(5) Ghenuche, P.; Cherukulappurath, S.; Quidant, R. *New J. Phys.* **2008**, *10*, 105013. Alegret, J.; Rindzevicius, T.; Pakizeh, T.; Alaverdyan, Y.; Gunnarsson, L.; Käll, M. *J. Phys. Chem.* **2008**, *112*, 14313–14317. Wustholz, K. L.; Henry, A.-I.; McMohan, M.; Freeman, R. G.; Valley, N.; Piotti, M. E.; Natan, M. J.; Scatz, G. C.; Van Duyne, R. P. *J. Am. Chem. Soc.* **2010**, *132*, 10903–10910.

(6) Hentschel, M.; Saliba, M.; Vogelgesang, R.; Giessen, H.; Alivisatos, A. P.; Liu, N. *Nano Lett.* **2010**, *10*, 2721–2726.

(7) Lassiter, J. B.; Sobhani, H.; Fan, J. A.; Kundu, J.; Capasso, F.; Nordlander, P.; Halas, N. J. *Nano Lett.* **2010**, *10*, 3184–3189.

(8) Fisher, U. C.; Dereux, A.; Weeber, J. C. *Near field optics and surface plasmon polaritons*; Topics in Applied Physics, 81; Springer: Berlin/Heidelberg, 2001.

(9) Girard, C.; Dujardin, E.; Baffou, G.; Quidant, R. *New J. Phys.* **2008**, *10*, No. 105016.

(10) Marty, R.; Arbouet, A.; Girard, C.; Margueritat, J.; Gonzalo, J.; Afonso, C. N. *J. Chem. Phys.* **2009**, *131*, No. 224707.

(11) Sepúlveda, B.; Angelomé, P. C.; Lechuga, L. M.; Liz-Marzán, L. M. *Nano Today* **2009**, *4*, 244–251.

(12) Matsubara, K.; Kawata, S.; Minami, S. *Appl. Opt.* **1988**, *27*, 1160–1163.

(13) Willets, K. A.; Van Duyne, R. P. *Annu. Rev. Phys. Chem.* **2007**, *58*, 267–297.

(14) Lin, V. K. X.; Teo, S. L.; Marty, R.; Arbouet, A.; Girard, C.; Alarcon-Llado, E.; Liu, S. H.; Han, M. Y.; Tripathy, S.; Mlayah, A. *Nanotechnology* **2010**, *21*, No. 305501.

(15) El-Sayed, I. H.; Huang, X.; El-Sayed, M. A. *Cancer Lett.* **2006**, *239*, 129–135.

(16) Liu, H.; Chen, D.; Tang, F.; Du, G.; Li, L.; Meng, X.; Liang, W.; Zhang, Y.; Teng, X.; Li, Y. *Nanotechnology* **2008**, *19*, No. 455101.

(17) Moskovits, M. *Rev. Mod. Phys.* **1985**, *57*, 783–826.

(18) Cao, Y. W. C.; Jin, R. C.; Mirkin, C. A. *Science* **2002**, *297*, 1536–1540.

(19) Jackson, J. B.; Halas, N. J. *Proc. Natl. Acad. Sci. U.S.A.* **2004**, *101*, 17930–17935.

(20) Huang, X.; El-Sayed, I. H.; Qian, W. I.; El-Sayed, M. A. *Nano Lett.* **2007**, *7*, 1591–1597.

(21) Huang, C. W.; Hao, Y. W.; Nyagilo, J.; Dave, D. P.; Xu, L. F.; Sun, X. K. *J. Nano Res.* **2010**, *10*, 137–148.

(22) Weitz, D. A.; Gramila, T. J.; Genack, A. Z.; Gersten, J. I. *Phys. Rev. Lett.* **1980**, *45*, 355–358.

(23) Fujii, M.; Nagareda, T.; Hayashi, S.; Yamamoto, K. *Phys. Rev. B* **1991**, *44*, 6243–6248. Fujii, M.; Nagareda, T.; Hayashi, S.; Yamamoto, K. *Phys. Rev. B* **1995**, *52*, 14273.

(24) Adichtchev, S.; Sirotkin, S.; Bachelier, G.; Saviot, S.; Etienne, S.; Stephanidis, B.; Duval, E.; Mermet, A. *Phys. Rev. B* **2009**, *79*, No. 201402.

(25) Nelet, A.; Crut, A.; Arbouet, A.; Del Fatti, N.; Vallee, F.; Portales, H.; Saviot, S.; Duval, E. *Appl. Surf. Sci.* **2004**, *226*, 209–215.

(26) Margueritat, J.; Gonzalo, J.; Afonso, C. N.; Mlayah, A.; Murray, D. B.; Saviot, L. *Nano Lett.* **2006**, *6*, 2037–2042.
(27) Large, N.; Saviot, L.; Margueritat, J.; Gonzalo, J.; Afonso, C. N.; Arbouet, A.; Langot, P.; Mlayah, A.; Aizpurua, J. *Nano Lett.* **2009**, *9*, 3732–3738.
(28) Bachelier, G.; Mlayah, A. *Phys. Rev. B* **2004**, *69*, No. 205408.
(29) Margueritat, J.; Gonzalo, J.; Afonso, C. N.; Hormann, U.; Van Tendeloo, G.; Mlayah, A.; Murray, D. B.; Saviot, L.; Zhou, Y.; Hong, M. H.; Luk'yanchuk, B. S. *Nanotechnology* **2008**, *19*, No. 375701.
(30) Girard, C. *Rep. Prog. Phys.* **2005**, *68*, 1883–1933.
(31) Romero, I.; Aizpurua, J.; Bryant, G. W.; García de Abajo, J. F. *Opt. Express* **2006**, *14*, 9988–9999.
(32) Zhang, W. H.; Huang, L.; Santschi, C.; Martin, O. J. F. *Nano Lett.* **2010**, *10*, 1006–1011.
(33) Søndergaard, T.; Tromborg, B. *Phys. Rev. B* **2002**, *66*, No. 155309.
(34) Lombardi, R. J.; Birke, R. L. *Acc. Chem. Res.* **2009**, *42*, 734–742.